

Benchmarking of Constant Power Generation Strategies for Single-Phase Grid-Connected Photovoltaic Systems

Sangwongwanich, Ariya; Yang, Yongheng; Blaabjerg, Frede; Wang, Huai

Published in:

Proceedings of the 31st Annual IEEE Applied Power Electronics Conference and Exposition (APEC)

DOI (link to publication from Publisher):

[10.1109/APEC.2016.7467899](https://doi.org/10.1109/APEC.2016.7467899)

Publication date:

2016

Document Version

Early version, also known as pre-print

[Link to publication from Aalborg University](#)

Citation for published version (APA):

Sangwongwanich, A., Yang, Y., Blaabjerg, F., & Wang, H. (2016). Benchmarking of Constant Power Generation Strategies for Single-Phase Grid-Connected Photovoltaic Systems. In *Proceedings of the 31st Annual IEEE Applied Power Electronics Conference and Exposition (APEC)* (pp. 370-377). IEEE Press.
<https://doi.org/10.1109/APEC.2016.7467899>

General rights

Copyright and moral rights for the publications made accessible in the public portal are retained by the authors and/or other copyright owners and it is a condition of accessing publications that users recognise and abide by the legal requirements associated with these rights.

- Users may download and print one copy of any publication from the public portal for the purpose of private study or research.
- You may not further distribute the material or use it for any profit-making activity or commercial gain
- You may freely distribute the URL identifying the publication in the public portal -

Take down policy

If you believe that this document breaches copyright please contact us at vbn@aub.aau.dk providing details, and we will remove access to the work immediately and investigate your claim.

Benchmarking of Constant Power Generation Strategies for Single-Phase Grid-Connected Photovoltaic Systems

Ariya Sangwongwanich¹, Yongheng Yang², *IEEE Member*, Frede Blaabjerg³, *IEEE Fellow*,
and Huai Wang⁴, *IEEE Member*

Department of Energy Technology
Aalborg University

Pontoppidanstraede 101, Aalborg, DK-9220 Denmark
ars@et.aau.dk¹, yoy@et.aau.dk², fbl@et.aau.dk³, hwa@et.aau.dk⁴

Abstract—With a still increase of grid-connected Photovoltaic (PV) systems, challenges have been imposed on the grid due to the continuous injection of a large amount of fluctuating PV power, like overloading the grid infrastructure (e.g., transformers) during peak power production periods. Hence, advanced active power control methods are required. As a cost-effective solution to avoid overloading, a Constant Power Generation (CPG) control scheme by limiting the feed-in power has been introduced into the currently active grid regulations. In order to achieve a CPG operation, this paper proposes three CPG strategies based on: 1) a power control (P-CPG), 2) a current limit method (I-CPG) and 3) the Perturb and Observe algorithm (P&O-CPG). However, the operational mode changes (e.g., from the maximum power point tracking to a CPG operation) will affect the entire system performance. Thus, a benchmarking of the proposed CPG strategies is also conducted on a 3-kW single-phase grid-connected PV system. Comparisons reveal that either the P-CPG or I-CPG strategies can achieve fast dynamics and satisfactory steady-state performance. In contrast, the P&O-CPG algorithm is the most suitable solution in terms of high robustness, but it presents poor dynamic performance.

Index Terms—Active power control, constant power control, maximum power point tracking, PV systems, power converters.

I. INTRODUCTION

Photovoltaic (PV) systems have a high growth rate during the last several years, and will play an even more significant role in the future mixed power grid [1]–[3]. Currently, a Maximum Power Point Tracking (MPPT) is mandatory for the PV systems in most active grid codes and also to ensure the maximum energy yield from the sun power [4]. At a high penetration level of PV systems in the near future, the grid may face a challenge of overloading during peak power generation periods through a day if the power capacity of the grid remains the same. For instance, it was reported by BBC that parts of the Northern Ireland's grid were overloaded by the increased number of grid-connected PV systems in a sunny and clear day [5]. In order to enable more PV installations and address such issues, the control algorithms have to be feasible to flexibly regulate the active power generated by PV systems [4], [6]–[8]. For instance, limiting the feed-in power of PV systems to a certain level has been found as a cost-effective approach to overcome overloading, and thus it is currently required in Germany through the grid codes [9]. Actually, this active power control strategy corresponds to an absolute power

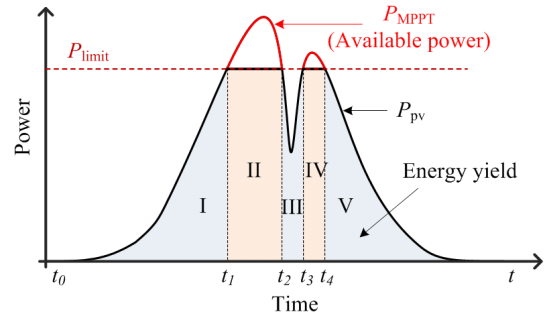


Fig. 1. Constant Power Generation (CPG) concept for PV systems: 1) MPPT mode during I, III, V, and 2) CPG mode during II, IV [13].

constraint defined in the Danish grid code [10], and is also referred to as a Constant Power Generation (CPG) control in prior-art work [11], [12].

According to [11], [13], the most intuitive and effective way to achieve the CPG control is through the modification of the MPPT algorithm at the PV inverter level. Specifically, as long as the PV output power P_{pv} is below the setting-point P_{limit} , the PV system continues operating in the MPPT mode with injection of the maximum power. However, when the output power reaches the level of P_{limit} , the PV system will inject a constant active power, i.e., $P_{pv} = P_{limit}$, by regulating the PV output power at the so-called Constant Power Point (CPP). The operational principle of the CPG scheme can be illustrated in Fig. 1 and

$$P_{pv} = \begin{cases} P_{MPPT}, & \text{when } P_{pv} \leq P_{limit} \\ P_{limit}, & \text{when } P_{pv} > P_{limit} \end{cases} \quad (1)$$

where P_{pv} is the PV output power, P_{MPPT} is the maximum available power (according to the MPPT operation), and P_{limit} is the power limit, which is the setting-point.

In the prior-art work, several CPG control strategies have been introduced. For example, in [14], a P&O based CPG algorithm has been used in single-stage three-phase PV systems. However, its operating region is limited due to the single-stage configuration. A conditioning switch to change the operating modes has been employed in [15] and [16], which requires the initialization of the controllers during the operational mode changes, while a compensation to stabilize the dc-link voltage

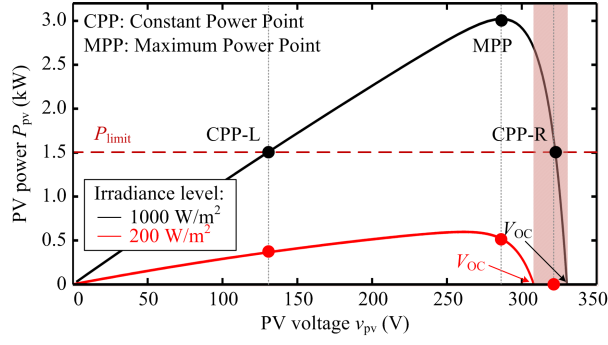


Fig. 2. Stability issues of the conventional CPG algorithms, when the operating point is normally located at the right side of the MPP for a PV panel system [12].

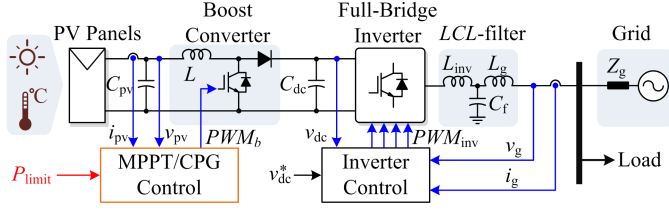


Fig. 3. Hardware schematics and overall control structure of a two-stage single-phase grid-connected PV system.

is needed in [17], and increasing the overall complexity. Additionally, most of the state-of-the-art CPG methods [14]–[17] cannot always ensure a stable operation (e.g., during a fast change in the irradiance), since the operating region is restricted to the right side of the Maximum Power Point (MPP) in the power-voltage (P-V) curve (i.e., at the CPP-R) shown in Fig. 2. In that region, the CPG operation can potentially introduce instability, since the operating point may go to the open-circuit condition when the PV systems experience a fast decrease of the irradiance condition [12].

In the light of the above issues, this paper proposes three CPG control methods for two-stage single-phase PV systems. The performances under both dynamic and steady-state conditions are benchmarked experimentally on a 3-kW two-stage single-phase PV system. Finally, conclusions are drawn on the comparison.

II. CONTROL STRUCTURE OF TWO-STAGE SINGLE-PHASE GRID-CONNECTED PV SYSTEMS

A. System Configuration

The system configuration and its control structure are shown in Fig. 3, where a two-stage single-phase grid-connected PV system is adopted. The system parameters are given in Table I. The PV arrays are connected to a boost converter, allowing a wide-range operation during both MPPT and CPG operations [18]. In other words, with the use of the boost converter, the PV system can operate at a lower PV voltage v_{pv} (e.g., at the left side of the MPP in the case of the CPG operation), since the PV output voltage v_{pv} can be stepped up to match the required dc-link voltage (e.g., 450 V) for the PV inverter [19].

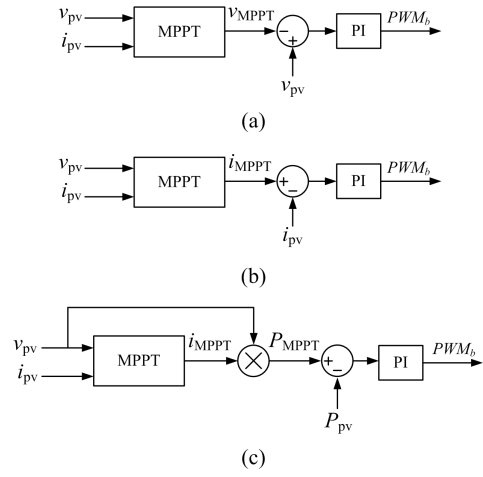


Fig. 4. Implementation of different MPPT controllers: (a) PV output voltage, (b) PV output current, and (c) PV output power, where PI represents a proportional-integral controller.

TABLE I
PARAMETERS OF THE TWO-STAGE SINGLE-PHASE PV SYSTEM (FIG. 3).

PV rated power	3 kW
Boost converter inductor	$L = 1.8$ mH
PV-side capacitor	$C_{pv} = 1000$ μ F
DC-link capacitor	$C_{dc} = 1100$ μ F
LCL-filter	$L_{inv} = 4.8$ mH, $L_g = 4$ mH, $C_f = 4.3$ μ F
Switching frequency	Boost converter: $f_b = 16$ kHz, Full-Bridge inverter: $f_{inv} = 8$ kHz
DC-link voltage	$V_{dc} = 450$ V
Grid nominal voltage (RMS)	$V_g = 230$ V
Grid nominal frequency	$\omega_0 = 2\pi \times 50$ rad/s

This may not be possible in the single-stage configuration, where the PV output voltage v_{pv} is directly fed to the PV inverter (i.e., $v_{pv} = v_{dc}$ with v_{dc} being the dc-link voltage). Practically, the v_{dc} is required to be higher than the grid voltage level (e.g., 325 V) to ensure the power delivery [20].

In the boost converter stage, either the MPPT or CPG control can be implemented in order to control the power extraction from the PV arrays. Then, the extracted power is delivered to the ac grid through the control of the full-bridge inverter. In this case, the control of the full-bridge inverter keeps the dc-link voltage to be constant through the control of the injected grid current [21].

B. Boost Converter Controller

As aforementioned, the boost converter plays a major role to control the power extraction from the PV arrays. Usually, the MPPT control (i.e., P&O MPPT algorithm) is implemented in the boost converter, which can be achieved by regulating the PV output voltage v_{pv} according to the reference voltage v_{MPPT} from the MPPT algorithm, as it is shown in Fig. 4(a). Actually, it is also possible to control the boost converter through the PV output current i_{pv} or the power P_{pv} [22] (e.g., Figs. 4(b) and (c)), which are of less robustness [23]. This is due to the

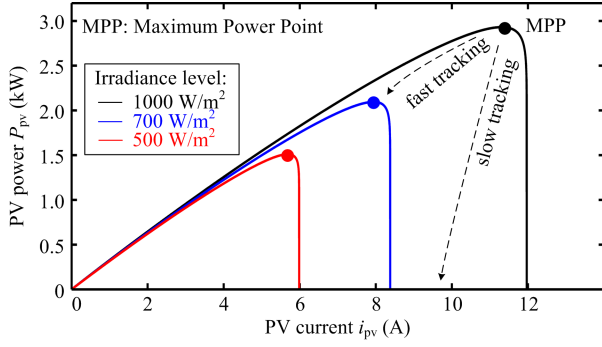


Fig. 5. Stability issues of the MPPT controller based on the PV output current due to the high slope (dP_{pv}/di_{pv}) at the right side of the MPP [23].

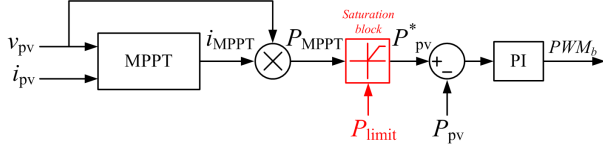


Fig. 6. Control structure of the Constant Power Generation (CPG) scheme based on a power control (P-CPG).

very steep slope (i.e., large dP_{pv}/di_{pv}) on the right side of the MPP in the power-current (P-I) curve of the PV arrays, as it is shown in Fig. 5. The operating point of the PV system may go into the short-circuit condition under a sudden decrease of the irradiance condition (if the MPPT algorithm cannot track fast enough), when the PV output current is controlled [23].

III. PROPOSED CONSTANT POWER GENERATION STRATEGIES

From the P-V characteristic curve of the PV arrays shown in Fig. 2, there are two possible operating points – CPP-L and CPP-R for the CPG mode at a certain power level (i.e., P_{limit}). Generally, the demands for the CPG control schemes are

- In the steady-state CPG operation, the CPG strategies should keep the PV systems operating at one of the CPPs with a minimum deviation, in order to minimize the power losses yield in the steady-state.
- Under a changing irradiance condition (e.g., in a cloudy day), the CPG control scheme should be able to track either the MPP or the CPP, depending on the operating mode, and at the same time ensure a stable transition.

Accordingly, three CPG strategies are proposed in the following based on: 1) a power control (P-CPG), 2) a current limit (I-CPG), and 3) the Perturb and Observe algorithm (P&O-CPG), where the above demands are taken as the benchmarking criteria.

A. CPG based on a Power Control (P-CPG)

As shown in Fig. 4(c), it is possible to directly control the PV output power P_{pv} by multiplying the reference current i_{MPPT} from the MPPT algorithm with the PV voltage v_{pv} . In order to achieve a CPG operation, the power reference P_{pv}^* is limited by using a saturation block, as it is shown in Fig.

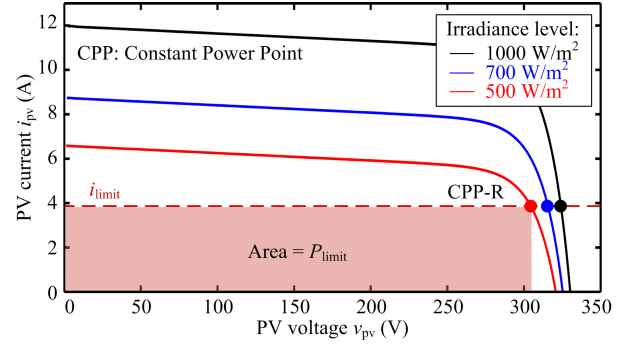


Fig. 7. Operational principle of the Constant Power Generation (CPG) scheme based on a current limit (I-CPG).

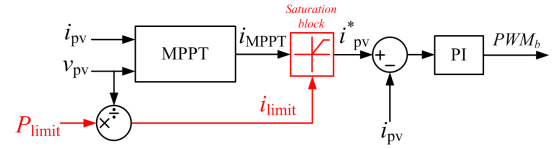


Fig. 8. Control structure of the Constant Power Generation (CPG) scheme based on a current limit (I-CPG).

6. Namely, when P_{MPPT} reaches the power limit P_{limit} , the power reference will be kept as a constant, i.e., $P_{pv}^* = P_{limit}$ and the PV system enters into the CPG mode. Otherwise, the PV system will operate in the MPPT mode with a maximum power injection (i.e., $P_{pv}^* = P_{MPPT}$). The operational principle can be further summarized as

$$P_{pv}^* = \begin{cases} P_{MPPT}, & \text{when } P_{MPPT} \leq P_{limit} \\ P_{limit}, & \text{when } P_{MPPT} > P_{limit} \end{cases} \quad (2)$$

where P_{MPPT} is the maximum available power (according to the MPPT operation), and P_{limit} is the power limit, as defined previously. Note that the P-CPG controller will regulate P_{pv} at the CPP-R, where the PV voltage v_{pv} is almost constant.

B. CPG based on a Current Limit (I-CPG)

Since the PV voltage v_{pv} is almost constant at the right side of the MPP (at the CPP-R), as it is shown in Fig. 7, the PV power P_{pv} can effectively be controlled through the PV current i_{pv} in this region. Thus, it is possible to achieve a CPG operation by limiting the reference current i_{MPPT} from the MPPT algorithm according to $i_{limit} = P_{limit}/v_{pv}$ [16], [17], as it is shown in Fig. 8. The power limit P_{limit} corresponds to the rectangular area under the CPP-R in Fig. 7.

According to the CPG concept in (1), the performance of the controller during the MPPT operation should not be diminished by the current limit. This can be ensured when considering

$$\frac{P_{MPPT}}{v_{pv}} \leq \frac{P_{limit}}{v_{pv}}$$

and thus,

$$i_{MPPT} \leq i_{limit}$$

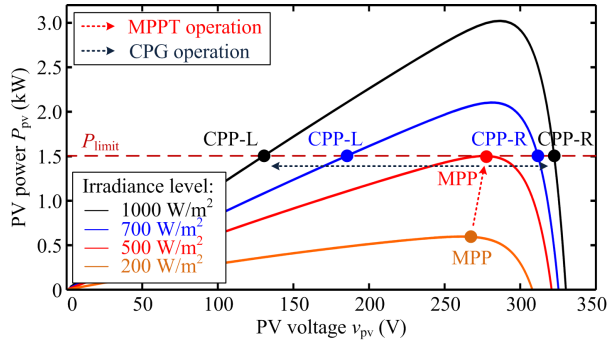


Fig. 9. Operational principle of the Constant Power Generation (CPG) scheme based on the P&O algorithm (P&O-CPG).

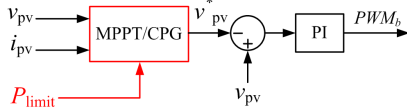


Fig. 10. Control structure of the Constant Power Generation (CPG) scheme based on the P&O algorithm (P&O-CPG).

where it can be seen that the current limit will not be activated as long as $P_{MPPT} \leq P_{limit}$.

C. CPG based on the P&O Algorithm (P&O-CPG)

A CPG operation can also be realized by means of a Perturb and Observe (P&O) algorithm. During the MPPT operation, the reference PV voltage v_{pv}^* is determined from the MPPT algorithm. However, in the case of the CPG operation, the PV voltage v_{pv} is continuously perturbed towards one CPP, i.e., $P_{pv} = P_{limit}$, as illustrated in Fig. 9. After a number of iterations, the operating point will be reached and oscillate around the corresponding CPP. Notably, the PV system with the P&O-CPG control can operate at either the CPP-L or the CPP-R, depending on the perturbation direction. However, the power oscillation in the steady-state is larger at the CPP-R compared to that at the CPP-L due to the high slope of the P-V curve on the right side of the MPP (i.e., large dP_{pv}/dv_{pv}). The control structure of the algorithm is shown in Fig. 10, where v_{pv}^* can be expressed as

$$v_{pv}^* = \begin{cases} v_{MPPT}, & \text{when } P_{pv} \leq P_{limit} \\ v_{pv} - v_{step}, & \text{when } P_{pv} > P_{limit} \end{cases} \quad (3)$$

if the PV system operates at the CPP-L, or

$$v_{pv}^* = \begin{cases} v_{MPPT}, & \text{when } P_{pv} \leq P_{limit} \\ v_{pv} + v_{step}, & \text{when } P_{pv} > P_{limit} \end{cases} \quad (4)$$

if the PV system operates at the CPP-R, where v_{MPPT} is the reference voltage from the MPPT algorithm (i.e., the P&O MPPT algorithm) and v_{step} is the perturbation step size.

IV. BENCHMARKING OF CONSTANT POWER GENERATION (CPG) STRATEGIES

In order to benchmark the discussed CPG control strategies, experiments have been carried out referring to Fig. 3, where

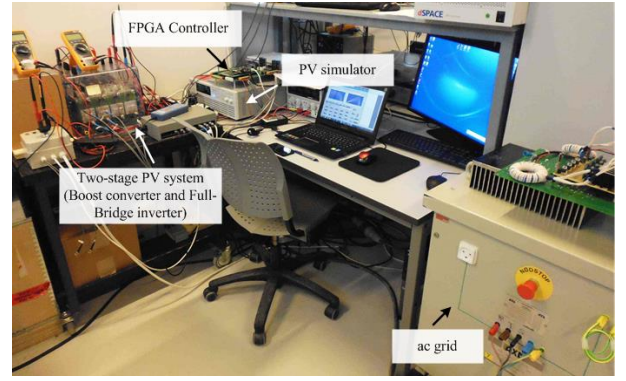


Fig. 11. Experimental setup of the two-stage single-phase grid-connected PV system.

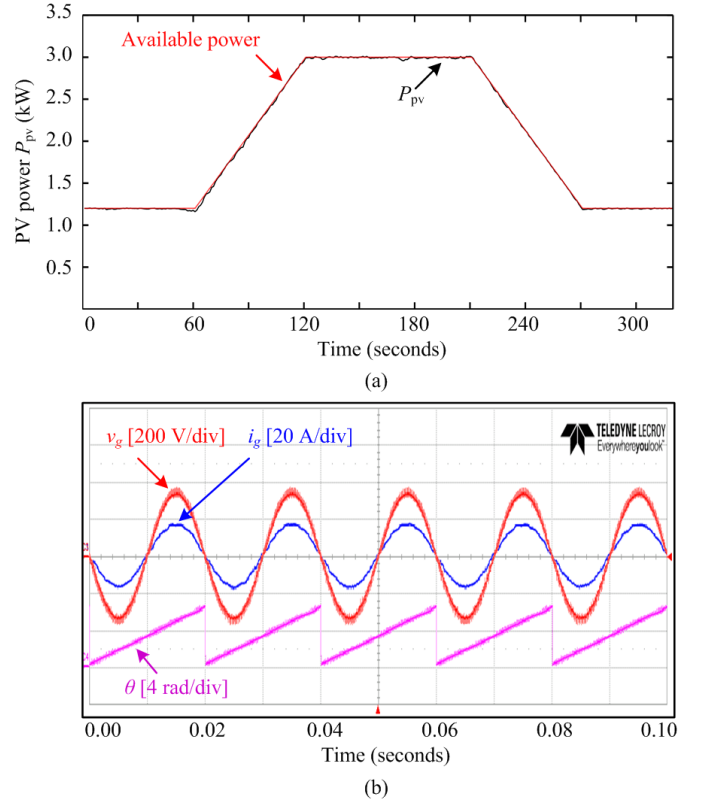


Fig. 12. Performance of the two-stage single-phase grid-connected PV system: (a) the PV power extraction during the MPPT operation, and (b) the grid voltage v_g , grid current i_g and the phase angle θ during the steady-state MPPT operation (3 kW).

the experimental test-rig is shown in Fig. 11. The performance of the two-stage single-phase PV system during the MPPT operation are demonstrated in Fig. 12(a). Here, the sampling frequency of the MPPT (and also CPG) algorithms is chosen as 10 Hz. For the PV inverter controller, the dc-link voltage v_{dc} is regulated at 450 ± 5 V and the extracted power is delivered to a single-phase 50-Hz ac grid with a peak voltage of 325 V, as it can be seen from Fig. 12(b).

In the experiments, a 3-kW PV simulator has been adopted,

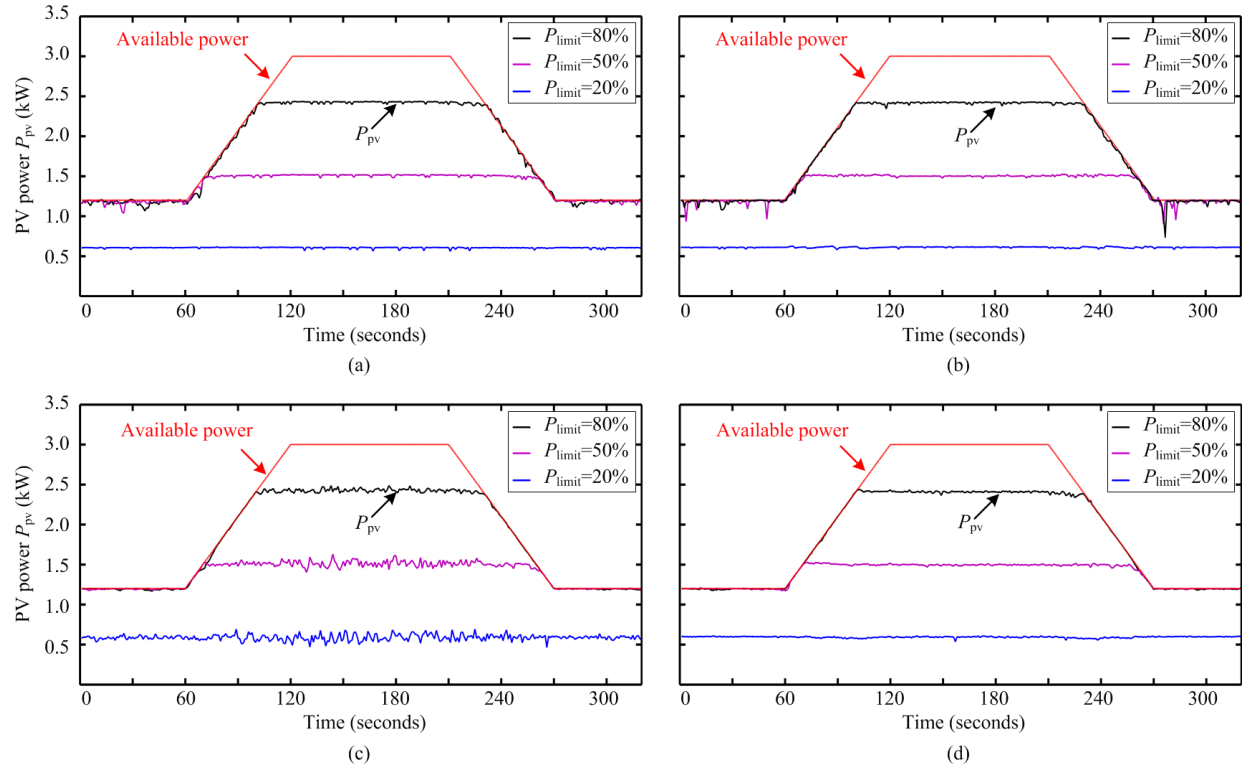


Fig. 13. Experimental results of the Constant Power Generation (CPG) scheme based on: (a) the power control, (b) the current limit, (c) the P&O at the right side of the MPP, and (d) the P&O at the left side of the MPP under a slow changing irradiance condition.

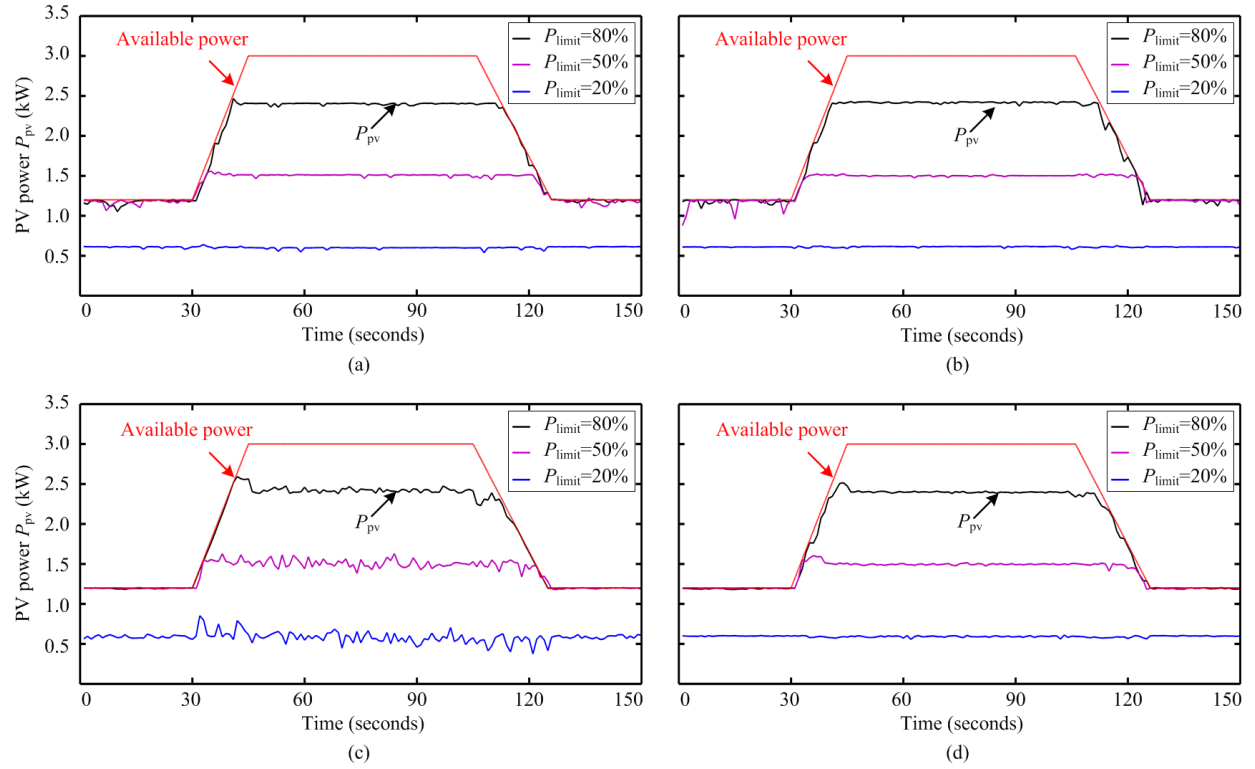


Fig. 14. Experimental results of the Constant Power Generation (CPG) scheme based on: (a) the power control, (b) the current limit, (c) the P&O at the right side of the MPP, and (d) the P&O at the left side of the MPP under a fast changing irradiance condition.

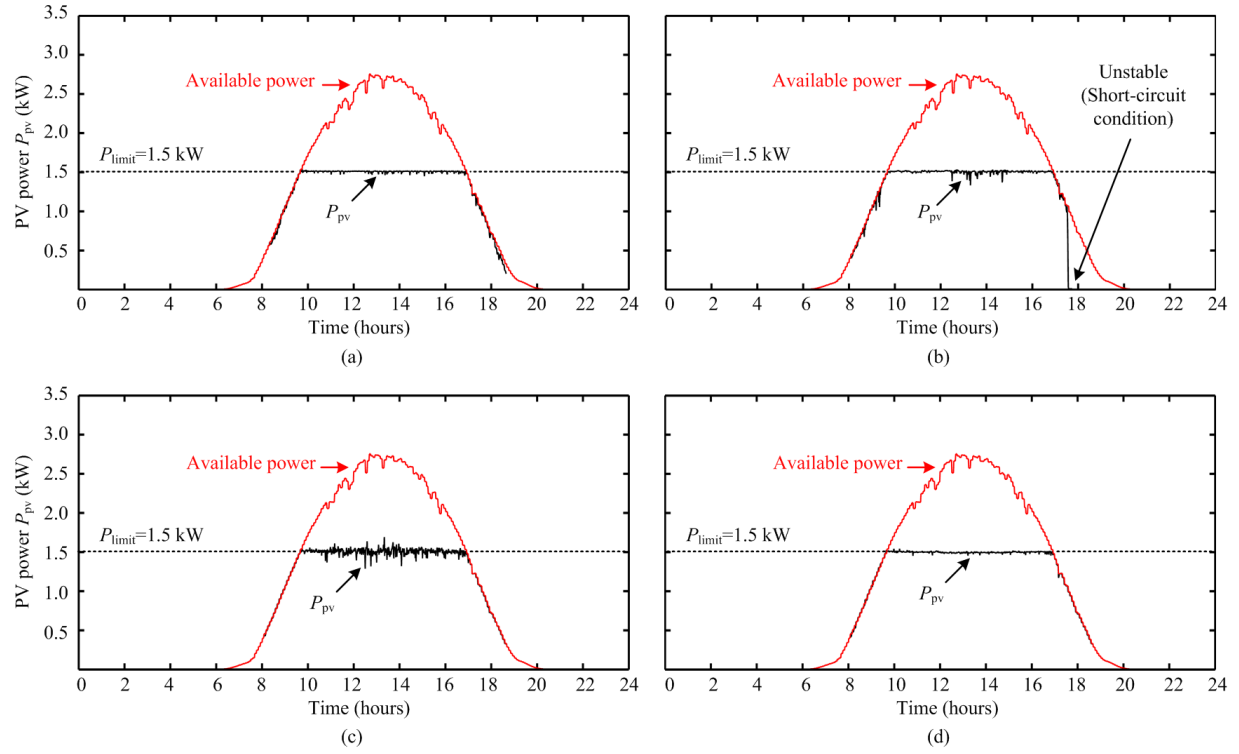


Fig. 15. Experimental results of the Constant Power Generation (CPG) scheme based on: (a) the power control, (b) the current limit, (c) the P&O at the right side of the MPP, and (d) the P&O at the left side of the MPP under a clear day condition.

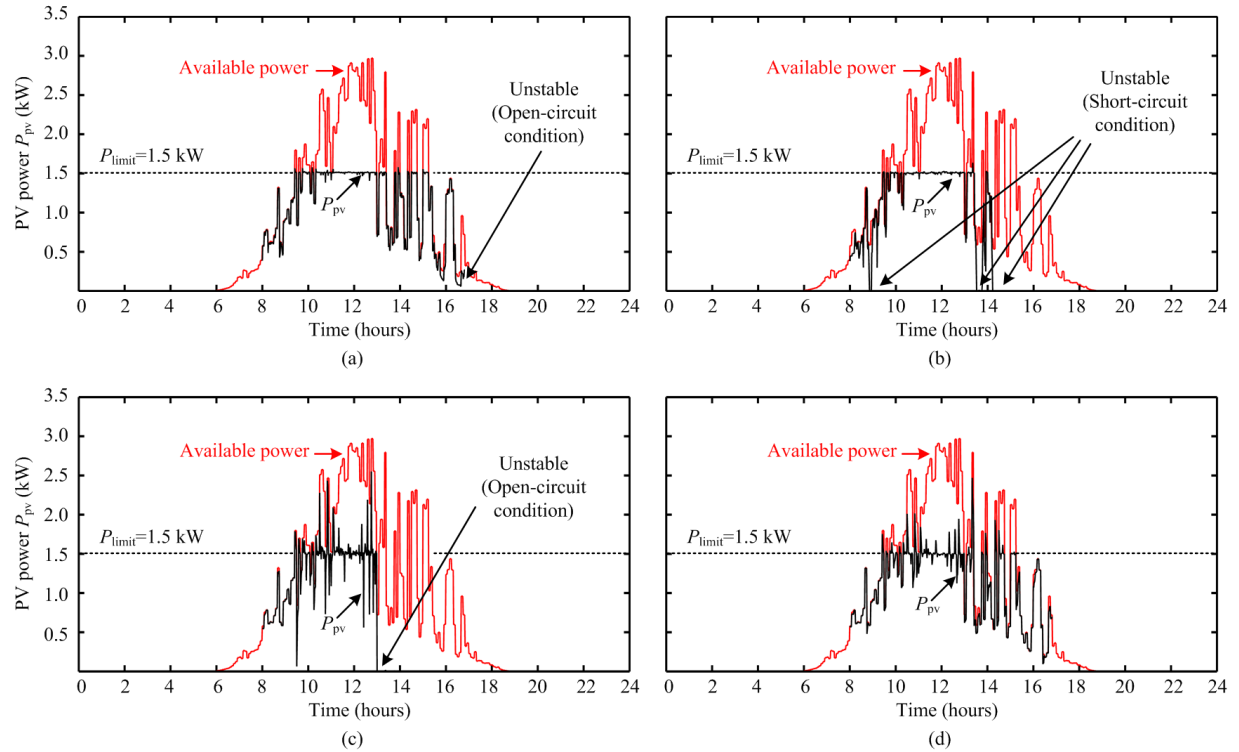


Fig. 16. Experimental results of the Constant Power Generation (CPG) scheme based on: (a) the power control, (b) the current limit, (c) the P&O at the right side of the MPP, and (d) the P&O at the left side of the MPP under a cloudy day condition.

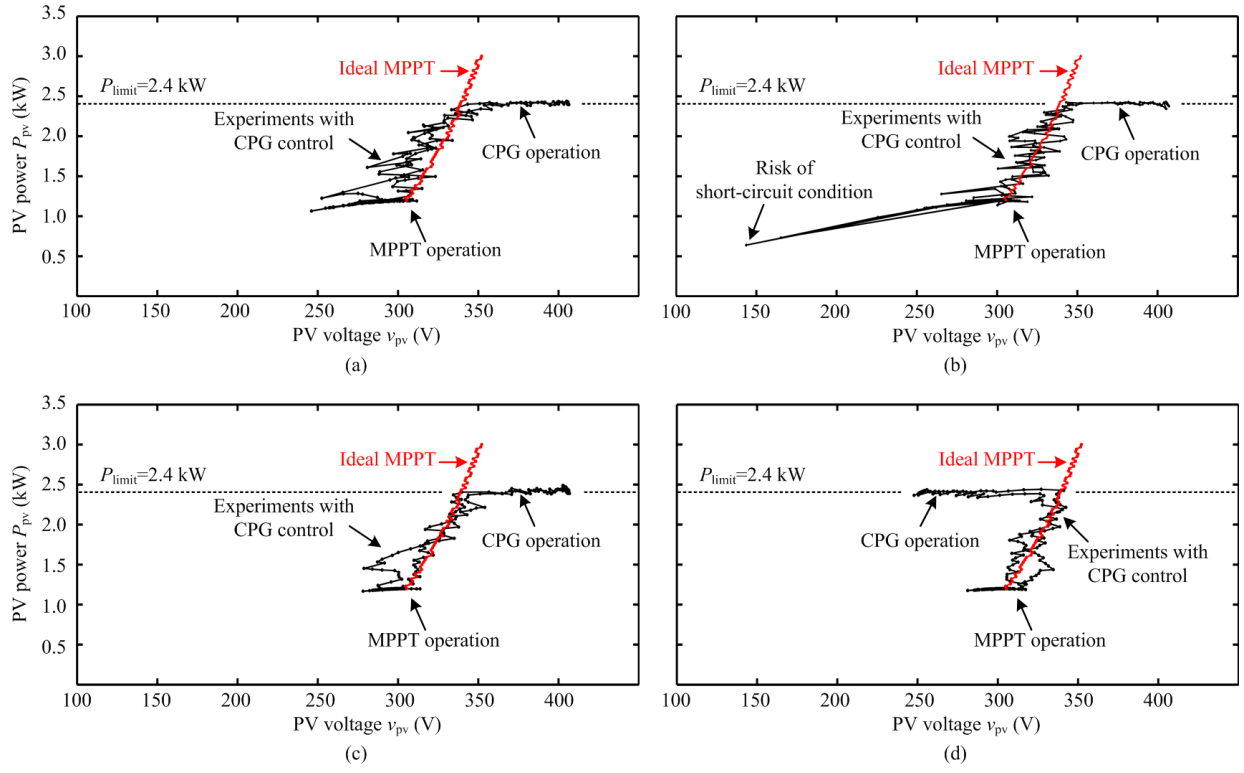


Fig. 17. Trajectory of the operating point of the Constant Power Generation (CPG) scheme based on: (a) the power control, (b) the current limit, (c) the P&O at the right side of the MPP, and (d) the P&O at the left side of the MPP under a slow changing irradiance condition (Fig. 13), when $P_{\text{limit}} = 2.4$ kW.

TABLE II
BENCHMARKING OF THE CONSTANT POWER GENERATION ALGORITHMS.

CPG Strategy	Dynamic Responses		Steady-state Responses	Stability	Complexity
	MPPT→CPG	CPG→MPPT			
Power control (P-CPG)	++	+	++	-	-
Current limit (I-CPG)	+	--	+	--	++
P&O-CPG at CPP-R	--	-	--	-	-
P&O-CPG at CPP-L	--	-	++	++	-

Note: the more +, the better stability and less complexity.

where two trapezoidal solar irradiance profiles are programmed in order to emulate a slow changing (i.e., Fig. 13) and a fast changing (i.e., Fig. 14) irradiance conditions. Here, three different values of power limit P_{limit} (i.e., 20, 50, and 80 % of the rated power) are used to confirm the feasibility of the CPG strategies. Furthermore, two real-field solar irradiance and ambient temperature profiles are also programmed in order to observe the performance of the CPG algorithms in the real operation, as it is shown in Figs. 15 and 16, where $P_{\text{limit}} = 1.5$ kW (i.e., 50 % of the rated power). An example of the operating trajectory of the CPG strategies are also illustrated in Fig. 17, where the irradiance condition in Fig. 13 is used.

A. Dynamic responses

The dynamic responses can be observed during the CPG to MPPT transition and vice versa. In Figs. 13 and 15, all the CPG strategies have a smooth transition, since the irradiance

changes relatively slow. However, in the case of fast changing solar irradiance, the P&O-CPG scheme presents large overshoots during the MPPT to CPG transition, as it is shown in Figs. 14 (c) and (d). Similar power overshoots also appear in the P&O-CPG algorithm under a cloudy day irradiance condition in Figs. 16 (c) and (d). In contrast, it is observed in Figs. 14 and 16 that the P- and I-CPG algorithms have a very fast dynamic response almost without any overshoots during the CPG transients.

B. Steady-state responses

In the steady-state, the CPG algorithm should regulate the PV power P_{pv} with minimum deviations, as discussed in § III. Most of the CPG algorithms have a satisfactory steady-state performance (see Figs. 13 and 15). However, when the P&O-CPG algorithm is employed to regulate the PV power at the right side of the MPP (i.e., the CPP-R), large power

oscillations appeared as shown in Figs. 13(c) and 15(c). This is due to the large dP_{pv}/dv_{pv} at the CPP-R (see Fig. 2).

C. Stability

Stability is another important aspect for the CPG control schemes. Thus, the proposed CPG strategies are also benchmarked in terms of stability. Instability can occur in the case of the P- and P&O-CPG algorithms when the operating point is chosen at the CPP-R. The operating point may go to the open-circuit condition if the PV power is regulated too far at the right side of the MPP, since the open-circuit voltage in the P-V curve decreases as the irradiance level drops. Figs. 16 (a) and (c) verify that the P-CPG or the P&O-CPG at the right side of the MPP can go into instability during transients. Furthermore, the I-CPG algorithm can also introduce instability to the PV system under a decreasing irradiance condition as it is shown in Figs. 15(b) and 16(b). However, in this case, it is due to the less robust MPPT schemes, which may result in a short-circuit condition, as it is explained in Fig. 5. In fact, it can be seen in Figs. 15 and 16 that the P&O-CPG algorithm can always ensure a stable operation regardless of the irradiance conditions, only when the PV system operating point is regulated at the CPP-L.

D. Complexity

When comparing all the above CPG strategies, it is found that the I-CPG algorithm has the simplest control structure, where only one additional current limiter needs to be added to the original MPPT controller in Fig. 4(b). Besides, the calculation of the i_{limit} is also simple by dividing P_{limit} by the measured PV voltage v_{pv} . The control structure of the P-CPG algorithm is more complicated, basically due to the MPPT controller in Fig. 4(c). In the case of the P&O-CPG algorithm, the modification needs to be done at the MPPT algorithm level as it can be seen from Fig. 10. This makes the design of a P&O-CPG controller more complicated than the other two CPG algorithms.

Table II further summarizes a comparison of the results of the proposed CPG control schemes, in terms of dynamic and steady-state performances, stability, and complexity. The benchmarking results have validated the effectiveness of the proposed CPG strategies, and that the P&O-CPG algorithm (when operating at the CPP-L) is the most suitable approach to realize the CPG control practically due to its robustness and feasible to be used for the future grid codes.

V. CONCLUSION

In this paper, three Constant Power Generation (CPG) control solutions for PV systems have been presented. A benchmarking of the three CPG control methods has also been conducted in terms of dynamic and steady-state performances, stability, and complexity. Comparisons have revealed that the CPG strategy based on a current limit (I-CPG) has the simplest control structure. Additionally, the power control based CPG scheme (P-CPG) has fast dynamics and good steady-state responses. However, instability may occur in both I-CPG and

P-CPG methods during the operational mode transition, e.g., in the case of a fast change in the solar irradiance. It can be concluded that the CPG based on the P&O algorithm (P&O-CPG) is the best one in terms of high robustness among the three CPG control strategies once the PV system is operating at the left side of the maximum power point.

REFERENCES

- [1] REN21, "Renewables 2015: Global Status Report (GRS)," 2015. [Online]. Available: <http://www.ren21.net/>.
- [2] Fraunhofer ISE, "Recent Facts about Photovoltaics in Germany," May 19, 2015. [Online]. Available: <http://www.pv-fakten.de/>.
- [3] Solar Power Europe, "Global Market Outlook For Solar Power 2015 - 2019," 2015. [Online]. Available: <http://www.solarpowereurope.org/>.
- [4] Y. Yang, P. Enjeti, F. Blaabjerg, and H. Wang, "Wide-scale adoption of photovoltaic energy: Grid code modifications are explored in the distribution grid," *IEEE Ind. Appl. Mag.*, vol. 21, no. 5, pp. 21–31, Sep. 2015.
- [5] D. Maxwell, "Parts of Northern Ireland's electricity grid overloaded," *BBC News NI*, 2013. [Online]. Available: <http://www.bbc.com/>.
- [6] T. Stetz, F. Marten, and M. Braun, "Improved low voltage grid-integration of photovoltaic systems in Germany," *IEEE Trans. Sustain. Energy*, vol. 4, no. 2, pp. 534–542, Apr. 2013.
- [7] A. Ahmed, L. Ran, S. Moon, and J.-H. Park, "A fast PV power tracking control algorithm with reduced power mode," *IEEE Trans. Energy Convers.*, vol. 28, no. 3, pp. 565–575, Sep. 2013.
- [8] T. Caldognetto, S. Buso, P. Tenti, and D. Brandao, "Power-based control of low-voltage microgrids," *IEEE Trans. Emerg. Sel. Topics Power Electron.*, vol. 3, no. 4, pp. 1056–1066, Dec. 2015.
- [9] *German Federal Law: Renewable Energy Sources Act (Gesetz für den Vorrang Erneuerbarer Energien) BGBI*, Std., Jul. 2014.
- [10] Energinet.dk, "Technical regulation 3.2.2 for PV power plants with a power output above 11 kW," Tech. Rep., 2015.
- [11] Y. Yang, H. Wang, F. Blaabjerg, and T. Kerekes, "A hybrid power control concept for PV inverters with reduced thermal loading," *IEEE Trans. Power Electron.*, vol. 29, no. 12, pp. 6271–6275, Dec. 2014.
- [12] A. Sangwongwanich, Y. Yang, and F. Blaabjerg, "High-performance constant power generation in grid-connected PV systems," *IEEE Trans. Power Electron.*, vol. 31, no. 3, pp. 1822–1825, Mar. 2016.
- [13] Y. Yang, F. Blaabjerg, and H. Wang, "Constant power generation of photovoltaic systems considering the distributed grid capacity," in *Proc. of APEC*, pp. 379–385, Mar. 2014.
- [14] R.G. Wandhare and V. Agarwal, "Precise active and reactive power control of the PV-DGS integrated with weak grid to increase PV penetration," in *Proc. of PVSC*, pp. 3150–3155, Jun. 2014.
- [15] W. Cao, Y. Ma, J. Wang, L. Yang, J. Wang, F. Wang, and L. Tolbert, "Two-stage PV inverter system emulator in converter based power grid emulation system," in *Proc. of ECCE*, pp. 4518–4525, Sep. 2013.
- [16] A. Urtasun, P. Sanchis, and L. Marroyo, "Limiting the power generated by a photovoltaic system," in *Proc. of SSD*, pp. 1–6, Mar. 2013.
- [17] Y. Chen, C. Tang, and Y. Chen, "PV power system with multi-mode operation and low-voltage ride-through capability," *IEEE Trans. Ind. Electron.*, vol. 62, no. 12, pp. 7524–7533, Dec. 2015.
- [18] H. Ghoddami and A. Yazdani, "A bipolar two-stage photovoltaic system based on three-level neutral-point clamped converter," in *Proc. IEEE Power Energy Soc. Gen. Meet.*, pp. 1–8, Jul. 2012.
- [19] S.B. Kjaer, J.K. Pedersen, and F. Blaabjerg, "A review of single-phase grid-connected inverters for photovoltaic modules," *IEEE Trans. Ind. Appl.*, vol. 41, no. 5, pp. 1292–1306, Sep. 2005.
- [20] B. Yang, W. Li, Y. Zhao, and X. He, "Design and analysis of a grid-connected photovoltaic power system," *IEEE Trans. Power Electron.*, vol. 25, no. 4, pp. 992–1000, Apr. 2010.
- [21] F. Blaabjerg, R. Teodorescu, M. Liserre, and A.V. Timbus, "Overview of control and grid synchronization for distributed power generation systems," *IEEE Trans. Ind. Electron.*, vol. 53, no. 5, pp. 1398–1409, Oct. 2006.
- [22] C. Rosa, D. Vinikov, E. Romero-Cadaval, V. Pires, and J. Martins, "Low-power home PV systems with MPPT and PC control modes," in *Proc. of CPE*, pp. 58–62, Jun. 2013.
- [23] N. Femia, G. Petrone, G. Spagnuolo, and M. Vitelli, *Power electronics and control techniques for maximum energy harvesting in photovoltaic systems*. CRC press, 2012.